Shi, Z., Lu, Z., and Chen, Q. 2019. "Indoor airflow and contaminant transport in a room with coupled displacement ventilation and passive-chilled-beam systems," *Building and Environment*, 161:106244.

Indoor Airflow and Contaminant Transport in a Room with Coupled Displacement Ventilation and Passive-chilled-beam Systems

Zhu Shi, Zechao Lu and Qingyan Chen*

School of Mechanical Engineering, Purdue University, West Lafayette, IN, USA

*Phone: (765) 496-7562, Fax: (765) 496-0539, Email: yanchen@purdue.edu

Abstract

Displacement ventilation (DV) is now widely used in enclosed environments such as office buildings. Although DV can provide good indoor air quality, its ability to remove heat is limited. On the other hand, passive chilled beams (PCBs) can have a high heat-removal capability. Therefore, this investigation evaluated a coupled DV and PCB system in terms of air quality and thermal comfort. This study first conducted experiments in a full-scale environmental chamber with the DV-PCB system to obtain airflow velocity, temperature and contaminant concentration data. A computational fluid dynamics (CFD) model was developed to simulate air distribution in an enclosed environment with the DV-PCB system, which was then validated by the measured data. The validated CFD model was employed to analyze thermal comfort and indoor air quality in the enclosed environment with the DV-PCB coupled system using four indices: vertical temperature gradient, draft rate, normalized contaminant concentration and age of air. The results indicate that PCBs were quite effective in reducing the temperature gradient created by DV. However, the cold downward jet generated by the PCBs created a "zone with high draft" under the PCBs, and the magnitude of the draft was strongly correlated with the cooling load removed by the PCBs and the size of the PCBs. In addition, the downward air jet generated by the PCBs could disrupt the contaminant stratification and increase the mean age of air in the occupied zone.

Keywords: Passive Chilled Beam, Displacement Ventilation, Thermal Comfort, Indoor Air Quality

Nomenclature

ACH	Air change per hour	$\Gamma_{\phi,eff}$	Turbulent diffusion coefficient
A_{PCB}	Total cross-sectional area of PCB used	T_s	Air temperature at supply
C	Contaminant concentration	T_{sp}	Setpoint temperature in room
C_e	Contaminant concentration at exhaust	t	Time
C_s	Contaminant concentration at supply	T_u	Turbulence intensity
C^*	Normalized contaminant concentration	u	Airflow velocity
H	Room height	u^*	Normalized velocity
h^*	Normalized height	x_i	Coordinates in i direction
I_{cl}	Clothing level	ΔT_{ha}	Air temperature difference between head and ankle
PD	Percentage dissatisfied people due to draft	θ	Normalized temperature
PMV	Predicted mean vote	ρ	Density

PPD	Percentage predicted dissatisfied people	τ	Mean age of air
Q_{PCB}	Load removed by PCB	η	Percentage of load removed by PCB
S_ϕ	Source	ν	Kinematic viscosity
T	Air temperature	ν_t	Turbulent eddy viscosity

1. Introduction

Maintaining good air quality and providing thermal comfort in indoor environments is not only critical for occupants' health, but is also important for their productivity at work [1]. An optimized heating, ventilation and air conditioning (HVAC) system is required to meet ventilation and thermal needs in an indoor space. Among the various HVAC systems, displacement ventilation (DV) has been thoroughly studied in the past forty years since its first application in Scandinavian countries. A typical DV system supplies clean air to the lower zone of the room and exhausts air near the ceiling, which creates a stratified air distribution. Previous researches [2,3,4,5] showed that such a system provides higher indoor air quality than a mixing ventilation (MV) system. For example, Xing and Awbi [2] measured contaminant concentration in rooms whose cooling loads varied from 10 W/m^2 to 60 W/m^2 and showed that thermal plumes in DV systems drew uncontaminated clean air from lower part and resulted in improved air quality at breathing zone. Gilani et al. [3] numerically simulated the mean age of air in indoor environments with DV systems and illustrated lower age of air in occupied zone than that in mixing zone, which demonstrated air quality benefits of DV. Mateus and da Graça [4] studied the performance of DV systems in a concert hall and found high CO_2 removal efficiencies of 1.2 to 1.7, which confirmed the air quality benefits of DV. Besides, other researches [6, 7, 8] also demonstrate energy saving potentials of DV systems. Lin et al. [6] performed a year-round energy analysis of DV applications in Hong Kong and concluded the energy saving could be over 25%, compared to MV systems. Ahmed et al. [7] explored the energy consumption in a room served by DV, and achieved an energy saving of more than 12.6% due to reduction in cooling coil load. In addition, the low supply-air velocity from DV diffusers ensures a low noise level [9, 10]. Because of these benefits of DV systems, they gained popularity in Scandinavia and U.S. and were promoted by ASHRAE by developed design guidelines [11, 12].

However, because DV supplies fresh air directly to the occupied zone, its supply-air temperature must not be too low. While supply air temperature in a MV system could be as low as 5 ^{o}C [10], Lau and Chen [13] indicated the supply air temperature in a DV system is normally higher than 16 ^{o}C. This feature limits the cooling capability, and hence the applicability, of DV. Furthermore, several studies [14, 15, 16, 17] have reported that a DV system, when used to remove a cooling load larger than 40 W/m^2, could create a large vertical temperature gradient in an occupied zone. This temperature gradient can cause thermal discomfort, which might. To create a more thermally comfortable environment and to enhance the ability to remove a high cooling load, remedies to these limitations of DV must be sought. Meanwhile, chilled beam systems are commonly used in indoor environments where cooling loads are high [18, 19, 20]. There are two types of chilled beam systems: active and passive. Compared with active chilled beams (ACB), passive chilled beams (PCB) are much less complex and less costly [21, 22]. Many studies have shown that PCBs can remove large cooling loads while saving energy. Fredriksson and Sandberg [23] demonstrated experimentally that a cooling efficiency (percentage of heat removed by the system) of 80% could be achieved by PCBs. Kim et al. [24] found that, depending on the climate zone, the use of PCBs resulted in energy savings between 8% and 24%, as compared to a variable air volume (VAV) system. Rumsey and Weale [25] and TIAX LLC [26] showed that chilled beams increased energy efficiency by 15% to 20% over conventional systems, since chilled beams use a higher chilled-

water temperature than that in traditional air-conditioning systems [27]. Hence, PCBs are a good candidate for coupling with DV in order to address the issue of low cooling ability. However, PCB produces a downward jet which could significantly change the local airflow velocity and temperature. Fredriksson and Sandberg [23] and Fredriksson et al. [28] used experimental methods to visualize and to measure such air jet beneath PCB, and found its magnitude could be as large as 0.28 m/s. Kosonen et al. [29] indicated that the jet induced by PCB might further affect the thermal comfort in occupied room space. In addition, a PCB can recirculate airborne contaminants near the ceiling downwards to the occupied zone, which could be counterproductive to the contaminant stratification produced by DV [30]. Therefore, a systematic study of the coupled DV-PCB system is needed, to evaluate its thermal and ventilation performance.

Studies of indoor air environments can take two approaches: experimental measurements and numerical simulations. Experimental measurements provide straightforward indoor air environment information such as airflow velocity and air temperature, but constructing the experimental apparatus and running experiments can be quite time-consuming and costly. Moreover, the dimensions of a test chamber are usually fixed, and thus the size of the investigated indoor space is limited [3 ,31, 32]. With the rapid development of computer processing power, the computational fluid dynamics (CFD) method has also been widely used in the investigation of indoor air environments. For instance, in some researches [3, 33, 34] it was used for predicting indoor airflow velocity and temperature. In other studies, it was also used to simulate air quality related parameters such as gaseous contaminant [35, 36, 37], volatile organic compound [38] or particle concentrations [39]. This method numerically solves the governing equations, and the results can provide a more comprehensive picture of the airflow at much lower cost than direct measurements. However, CFD uses models to approximate flow and heat transfer physics, which could lead to errors [40, 41]. Hence, it is vital that experimental data be used to validate CFD results and that the appropriate approximations are used in the CFD method.

This study first constructed a coupled DV-PCB system in a full-scale environmental chamber to measure airflow velocity, air temperature and airborne contaminant concentration. A CFD model was also developed to simulate the airflow in this coupled system, and the simulated results were validated by the measurement data. The validated CFD model was used both to depict the indoor airflow characteristics in the coupled system, and to quantify the thermal and ventilation impacts of PCBs on the DV system. Finally, this study proposed preliminary recommendations for the design of DV-PCB systems on the basis of the analysis results.

2. Research Methods

This investigation used experimental measurements to obtain data for validating a CFD model and employed the CFD model to analyze the air distribution for rooms with DV-PCB systems. This section details the experimental method and the CFD model.

2.1 Experimental Measurements

2.1.1 Test chamber

In order to obtain high-quality experimental data for validating the CFD model, this study constructed a coupled DV-PCB system in an environmental chamber as shown in Fig. 1. The chamber had dimensions of 6.08 m in length, 5.15 m in width, and 3.05 m in height. In this chamber, fresh air was supplied through two diffusers located at floor level at the corners of one of the side walls, and exhausted through an outlet on the opposite wall near the ceiling. The chamber contained tables; heated boxes with dimensions of 0.41 m × 0.41 m × 1.13 m and 84 W power, each simulating a seated person; and heated boxes with dimensions of 0.41 m × 0.25 m × 0.51 m and 109 W power, each simulating a personal computer (PC). Heat was generated by light bulbs installed inside these

boxes, and mini-fans were used to stir the inside air, so that the heated air could circulate. On the ceiling of the chamber, there were four lights. The number and locations of the above items could be changed, and thus the environmental chamber could be used to simulate different cooling loads and various room layouts. For example, Fig. 2(a) illustrates an office layout where simulated occupants are seated back to back at tables, Fig. 2 (b) shows a classroom layout where simulated occupants are facing the same direction, and Fig. 2(c) is a conference room layout in which simulated occupants sit around tables. The circled numbers in the figure are the locations for measuring the air parameters.

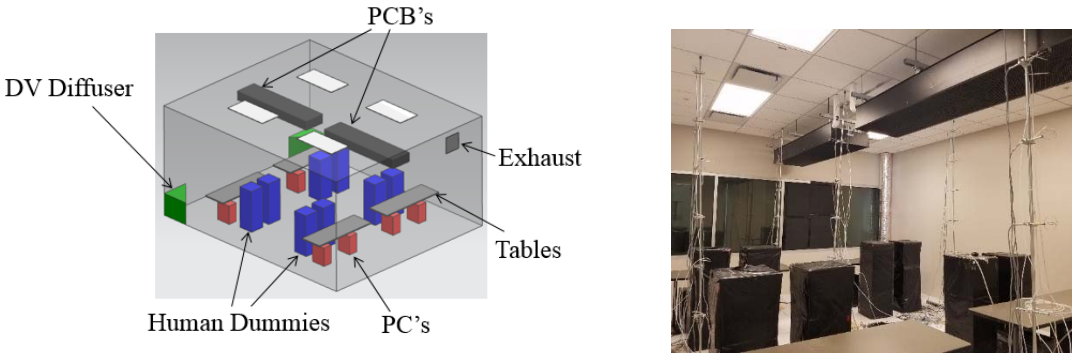

(a) 3D geometry of items inside chamber

(b) Photograph of environmental chamber

Fig. 1 Environmental chamber

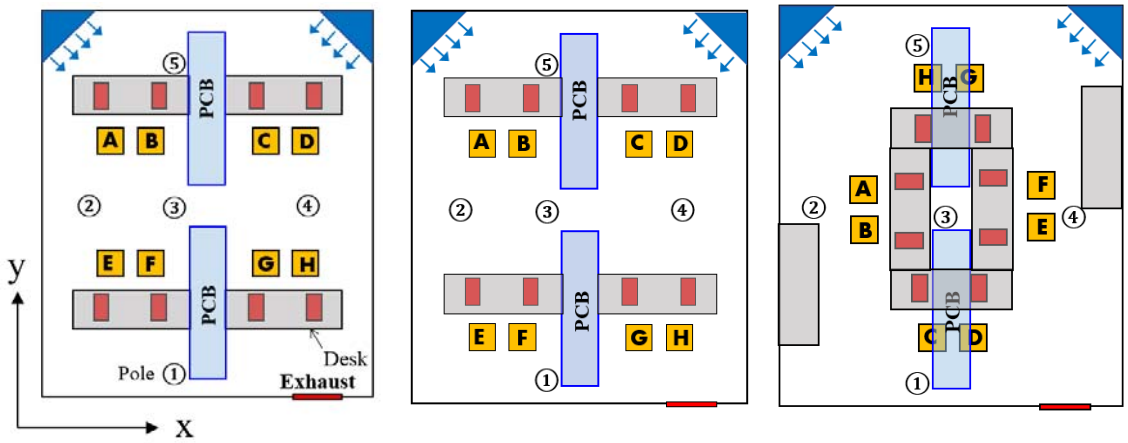

(a) Office layout (b) Classroom layout (c) Conference room layout

Fig. 2 Room layouts and measurement locations (yellow boxes: human dummies; red boxes: PC's; grey boxes: tables; circled numbers: measuring pole locations)

2.1.2 Air handling system and PCBs

Fig. 3(a) shows the air handling system of the environmental chamber, including a cooling coil, two heaters and two variable-speed fans. With the use of these components and control software, the supply-air flow rate and temperature could be adjusted as needed. Fig. 3(b) is the plumbing system for the PCBs that were installed inside the chamber. Chilled water was supplied from a water reservoir to beams. For each PCB, a flowmeter (OMEGA FTB-101, with ±0.1% accuracy) was used to monitor the water flow rate, which could be varied by turning the valve. Meanwhile, supply and return water temperatures for each PCB were measured. The water temperature could

also be adjusted in the building automation system. In this study, the supply water temperature was controlled in the range of 12–18°C, and the maximum waterflow rate for each beam was 13 L/min. By combining water supply temperature, return temperature and flow rate, one can calculate and adjust the heat removal rate for each PCB.

Fig. 3(c) and Fig. 3(d) show a photograph and a 3D model of a typical PCB, respectively. Sheet metal encloses cooling coils on four sides, while air can enter the PCB through the top surface and exit through the bottom. Detailed dimensions of PCBs vary from manufacturer to manufacturer. This study used three types of PCB (labeled A, B and C) made by three different companies, and Table 1 lists their dimensions.

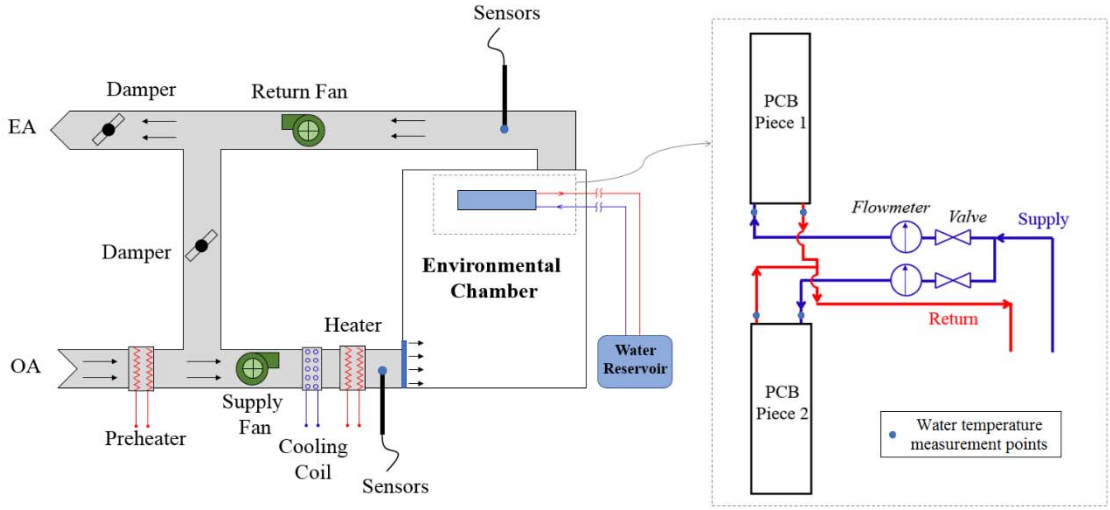

(a) Air handling system (b) Chilled water supply to PCB

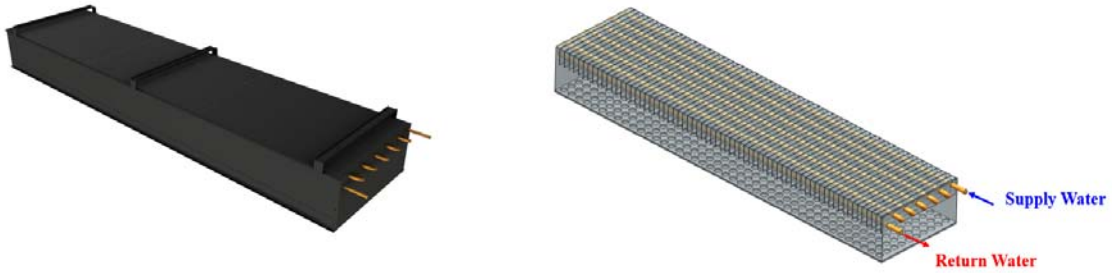

(c) Photograph of a typical PCB (d) 3D model of detailed geometry of a PCB

Fig. 3 Schematic of coupled DV and PCB system

Table 1. Dimensions of the three types of PCB investigated in this study

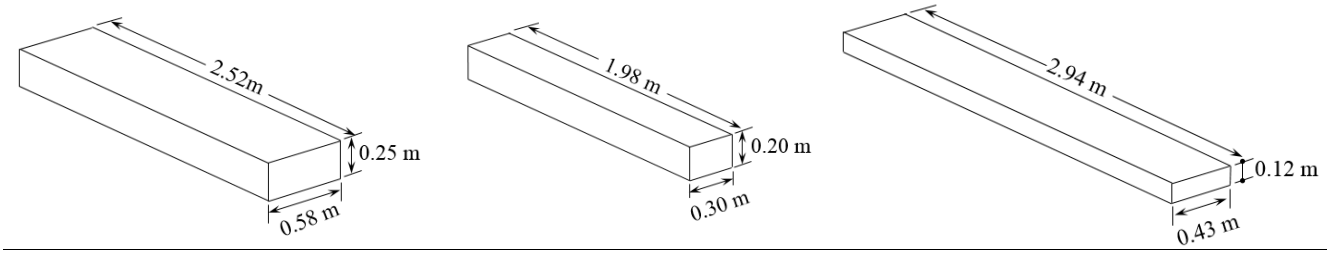

Type A Type B Type C

2.1.3 Experimental instruments and methods

Airflow velocity, air temperature and contaminant concentration are important pieces of information in regard to indoor air quality and thermal comfort, and were thus measured in the current study. Airflow velocity and temperature were measured using hot-sphere anemometers, the accuracy of which was ± 0.01 m/s for velocity and ± 0.3°C for temperature. The hot-sphere anemometers have measurement frequencies of 1 Hz. This investigation released a tracer gas (sulfur hexafluoride, or SF_6) above a simulated occupant to simulate contaminant emission by the occupant, and measured the tracer-gas concentration in the chamber using a multi-point sampler [42] and a photoacoustic multi-gas analyzer [43], with minimum reading of 0.01 ppm. Measurements were conducted along 5 poles that were evenly distributed throughout the chamber, with 7 measurement heights on each pole. The distance between adjacent measurement locations on the same pole was 0.46 m. This study also used an infrared thermometer (with reading repeatability of $\pm 0.02\%$ of absolute temperature) to measure surface temperatures. Before each set of measurements, this investigation operated the HVAC system for more than two hours to reach a steady state.

During the experiment, three computers (1, 2 and 3) were placed outside of chamber for experimental operation and data collection. Computer 1 was used to control air handling and PCB systems via a building automation system. Computer 2 was for reading airflow velocity and temperature results through a LabView program. Computer 3 was set up for obtaining SF_6 concentration readings. All the operations and data monitoring were performed in a non-intrusive way in order not to affect airflow and contaminant concentration inside chamber.

2.2 CFD Modeling

To predict the airflow velocity, air temperature and contaminant concentration in the room, this study developed a CFD model that employed Reynolds-Averaged Navier Stokes (RANS) equations with the Re-Normalized Group (RNG) $k-\varepsilon$ model [44]. This turbulence model was adopted because it had been recommended for predicting indoor airflow [45]. With the use of this model, the transport equations for mean values were generalized as:

$$\rho\frac{\partial\langle\phi\rangle}{\partial t}+\rho\langle u_i\rangle\frac{\partial\langle\phi\rangle}{\partial x_i}-\frac{\partial}{\partial x_i}\left[\Gamma_{\phi,eff}\frac{\partial\langle\phi\rangle}{\partial x_i}\right]=S_\phi \qquad (1)$$

where ϕ could represent velocity components $u_i\,(i=1,2,3)$, turbulent kinetic energy k, turbulent dissipation rate ε, energy E, or contaminant concentration C. The S_ϕ and $\Gamma_{\phi,eff}$ stand for the source term and effective diffusion coefficient of scalar ϕ, respectively. The Boussinesq approximation was used to account for the variation in air density with temperature. One can refer

to ANSYS Inc. [46] for more details about this turbulence model and the Boussinesq approximation.

Proper specification of boundary conditions and appropriate establishment of mesh structure are important for accurate simulation of indoor airflow and contaminant transportation by a CFD model. In this study, non-slip boundary conditions were prescribed on surfaces of heated objects as well as walls. The surface temperatures were obtained from measurements. Each piece of the PCB was modeled as an energy sink [47]. The corresponding heat absorption rate per unit volume was calculated from the heat removal rate and the volume of the PCB. The SF_6 source was assumed to have zero momentum since the release amount was minimal. Fig. 4 illustrates the mesh structure for this study. A combination of structured and unstructured meshes was used to discretize the computational domain. Inflation layers of structured meshes were employed to capture the relatively large temperature gradients around heated surfaces, while unstructured meshes were used to handle the complicated interior geometry. This study performed a grid-independence study with three grid resolutions: 0.89 million (coarse), 3.51 million (medium) and 8.42 million (fine). The results indicated that a mesh with 3.51 million cells was sufficient to capture the airflow features in the room. Examination of the average velocity magnitudes in a $0.2m \times 0.2m \times 0.2m$ air box beneath PCB showed the difference between results in the "coarse" case and "medium" case was 17%, and that between "medium" case and "fine" case was less than 5%. The corresponding grid size from "medium" case was thus used for further study.

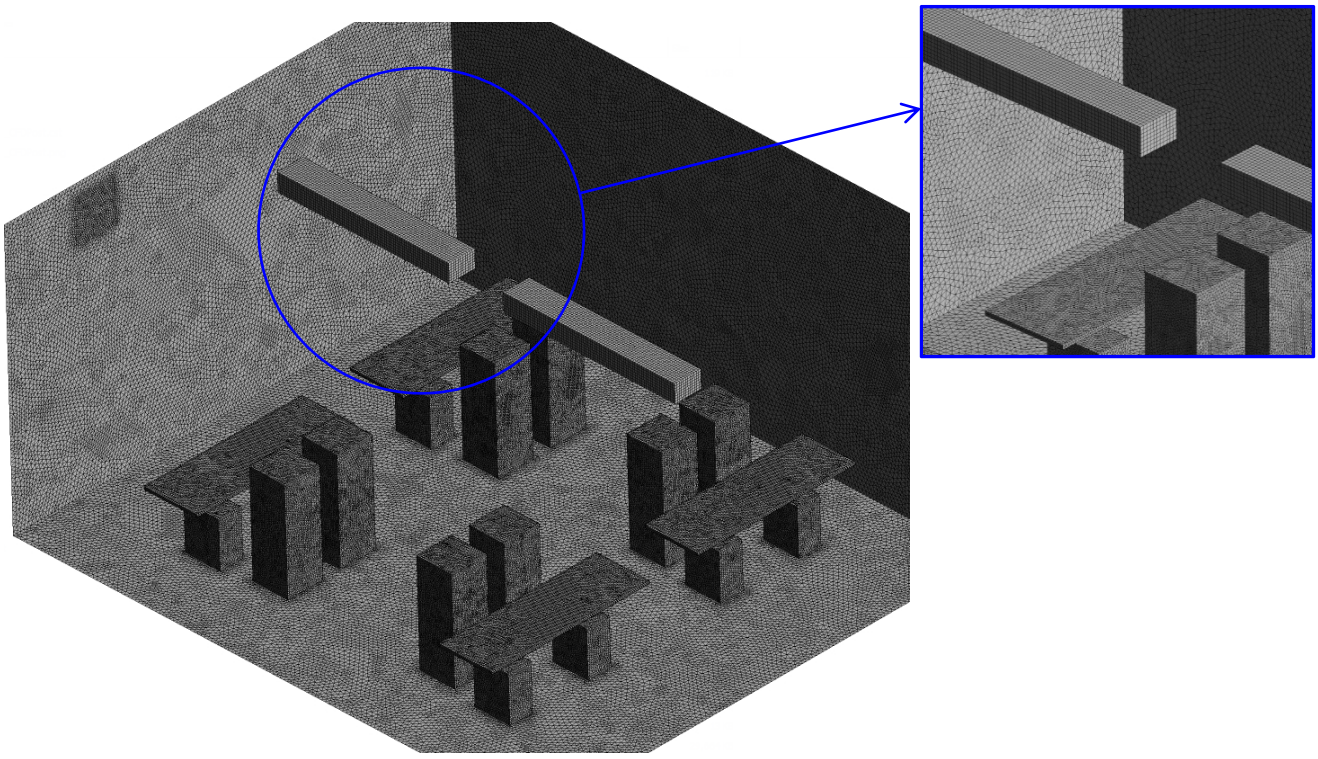

Fig. 4 Mesh structure in the CFD model

This study employed a commercial CFD program, ANSYS Fluent 17.0 [46], to calculate airflow and contaminant transport. The semi-implicit method for pressure-linked equations (SIMPLE) algorithm was adopted to couple velocity and pressure equations. The second-order method was used to spatially discretize u_i, k, ε, C and E. This study considered the simulation to be

converged when normalized residuals were less than 10^{-6} for E and less than 10^{-4} for the u_i, k, ε and C terms. The airflow velocity, air temperature and contaminant concentration results from the CFD model were then compared with the experimental data.

2.3 Indices for evaluating thermal comfort and indoor air quality

The above experimental measurements and CFD model were used to obtain airflow and contaminant distribution information. To appraise the performance of the DV-PCB system, this study employed the following indices to quantitively evaluate the resulting thermal comfort and air quality.

2.3.1 Thermal comfort indices

According to the literature [48, 49, 50], the vertical air temperature difference between head and ankle creates thermal discomfort for occupants. Therefore, this study examined the temperature difference:

$$\Delta T_{ha1} = T_{1.1\mathrm{m}} - T_{0.1\mathrm{m}},\ \Delta T_{ha2} = T_{1.7\mathrm{m}} - \mathrm{T}_{0.1\mathrm{m}} \tag{1}$$

where ΔT_{ha1} and ΔT_{ha2} represent temperature gradients for a seated and standing occupant, respectively. ASHRAE [51] recommends that ΔT_{ha1} be lower than 2 K, and that ΔT_{ha2} be lower than 3 K.

Furthermore, unwanted cooling of the body caused by air movement leads to a draft sensation [52]. This study used the following equation to predict the percentage of people dissatisfied due to draft:

$$PD = (34 - T)(u - 0.05)^{0.62}(3.14 + 0.37uT_u), \tag{2}$$

where u is mean velocity, T is temperature, and T_u is the local turbulence intensity [52].

2.3.2 Air quality indices

The normalized contaminant concentration, C^*, was employed to evaluate air quality in the room [53]. It is defined as:

$$C^* = \frac{C - C_s}{C_e - C_s} \tag{3}$$

where C, C_e and C_s are the contaminant concentration at a particular location, at the exhaust, and at the supply, respectively. When the room is in a perfectly mixed condition, C^* is equal to 1.

In addition, this study investigated the local mean age of air (MAA), τ, which is the average time needed for air to travel from the inlet to a specific location in the room [33, 54]. This τ is not a pre-defined variable in ANSYS Fluent, but, according to its definition, it can be obtained by solving:

$$\rho\frac{\partial \tau}{\partial t} + \rho\langle u_i\rangle\frac{\partial \tau}{\partial x_i} - \frac{\partial}{\partial x_i}\left[\Gamma_{\tau,eff}\frac{\partial \tau}{\partial x_i}\right] = \rho \tag{4}$$

where the effective diffusion coefficient is given by:

$$\Gamma_{\tau,eff} = \rho\nu + \nu_t/0.7 \tag{5}$$

These indices both contain information about indoor air quality, but they evaluate air quality from different perspectives: $C*$ indicates the contamination level of room air when contaminant is released in the room, whereas τ is a direct measure of the freshness of room air.

3. Results

We first used measured data to validate the developed CFD model. The validated model was then employed to study the characteristics of PCB-induced airflow in an indoor space, to analyze thermal comfort levels, and to assess the ventilation performance of a DV-PCB system.

3.1 Model validation

To ensure that the CFD model yielded accurate predictions that could be used for further analysis, this investigation first used experimental results to validate the model. We collected a large amount of measurement data. However, because of the space limitations in this paper, we have used the results only from Poles 1, 2 and 5 for a representative case (61 W/m^2, 40% of cooling load removed by two pieces of type B PCB) for the validation. The locations of these poles are shown in Fig. 2. Meanwhile, Fig. 5 illustrates the airflow velocity, temperature and contaminant concentration from the experiment and the simulation, with the values normalized as:

$$h^* = h/H,\ u^* = u/U,\ \theta = (T - T_s)/(T_e - T_s),\ C^* = (C - C_s)/(C_e - C_s) \qquad (6)$$

where H, T_s and T_e represent room height, supply air temperature and exhaust air temperature, respectively. Here U is a constant velocity of 0.2 m/s.

As shown in Fig. 5(a), the airflow velocity in the lower part of room was generally higher than that in the upper part. This difference was due to two factors. First, the DV system supplied fresh air to the lower part of room. This was the main reason for the high air velocity along Pole 2 (close to the DV diffusers) at ground level. Second, the downward jet generated by the PCBs impinged with objects in the occupied zone and increased the local air velocity. Fig. 5(b) further depicts the air velocity development beneath a PCB. The mean airflow velocity under the PCB started at a small magnitude but increased continuously until it reached a peak. This increase can be explained by the entrainment effect that drew ambient air to the jet center [55, 56]. The airflow velocity then gradually decayed as a result of dissipation of airflow momentum and jet impingement with the objects in the occupied zone. Fig. 5(c) shows the normalized temperature distributions along the three poles. Although the PCBs created a downward cold jet that caused local mixing, there still existed a temperature gradient in the bulk region because of the thermal plume. Finally, as shown in Fig. 5(d), when PCBs were used, they could disrupt the contaminant stratification generated by DV.

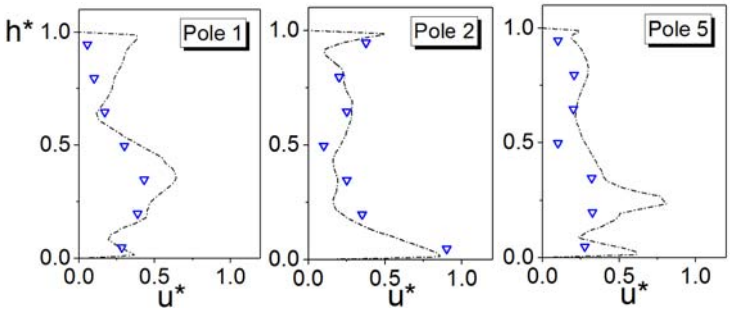

(a) Normalized velocity

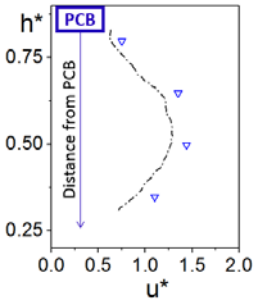

(b) Normalized velocity under a PCB

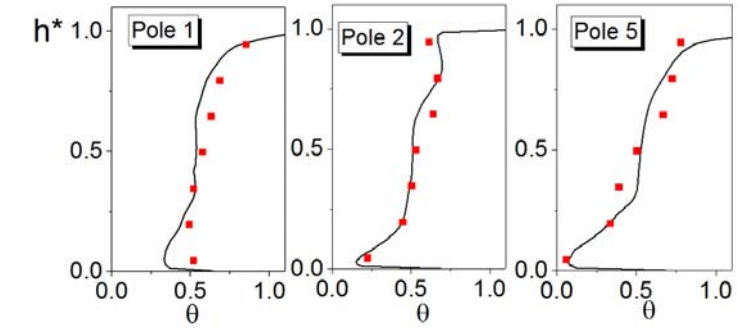

(c) Normalized temperature under PCBs

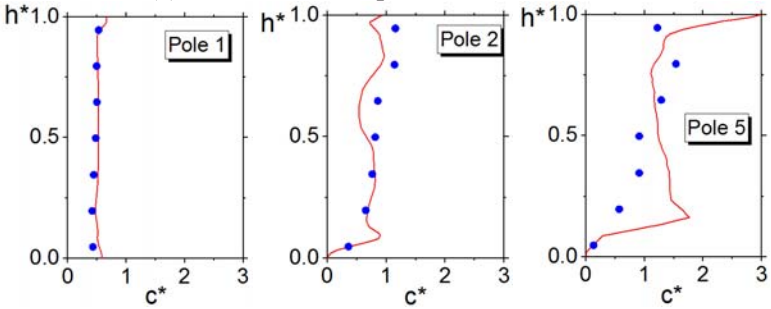

(d) Normalized contaminant concentration

Fig. 5 Airflow velocity, temperature and contaminant distributions in a DV-PCB system (Symbols: experimental data; lines: simulation data.)

The relative errors between the simulation and experimental results for the air velocity, temperature and contaminant concentration were 26.9%, 14.4% and 20.9%, respectively. The discrepancies can be explained in part by the uncertainties in the measurement positions. The errors caused by such uncertainties may have been particularly significant in locations where the variable gradient was large, such as the SF_6 concentration along Pole 5. Besides, SF_6 transport in the room is quite sensitive to local airflow, which might lead to noticeable local discrepancy between simulation and measurement in SF_6 concentration prediction. In fact, discrepancy of this kind was also reported in previous indoor airflow and contaminant transport simulation works [31, 41]. Furthermore, the CFD model employed a large number of approximations in discretization and turbulence modeling and these approximations could also have contributed errors. However, the overall trends in air velocity, temperature and contaminant concentration were still predicted with reasonably good accuracy. Therefore, the CFD model was considered validated and was used for further analysis.

3.2 Characteristics of airflow induced by PCBs

Using the validated CFD model, this study examined the airflow characteristics around a PCB, as illustrated in Fig. 6. The air inside the PCB was cooled and thus became denser. As a result, the air dropped and generated a downward jet. Depending on its strength, the jet may have reached the floor, or its velocity may have decayed to zero in mid-air. Meanwhile, if heat sources such as dummies were placed at a sufficiently large distance from the PCB, the thermal plumes generated by these heat sources could still have ascended without being affected by the downward jet from the PCB. Besides, the airflow patterns show that if thermal plumes draw gaseous contaminants from occupied zone into upper part, it could be recirculated downwards by PCB-induced air jet, since gaseous contaminant passively follows indoor airflow.

Fig. 6(b) also depicts the air temperature contour in the vicinity of the PCB. Warmer air was drawn toward the top of the PCB and was cooled significantly when it passed through the PCB. The cold downward jet discharged from the PCB entrained the ambient air, which was warmer than the air

in the center of the jet. Consequently, the temperature at the jet center continued to increase along the centerline as the air in the jet core mixed with the entrained air. Since the temperature of the air jet was still lower than the ambient, the jet then cooled the air in the breathing zone through convection. With the use of the CFD model the mechanisms of PCB influence on local airflow and cooled indoor air were visualized and were thus better understood.

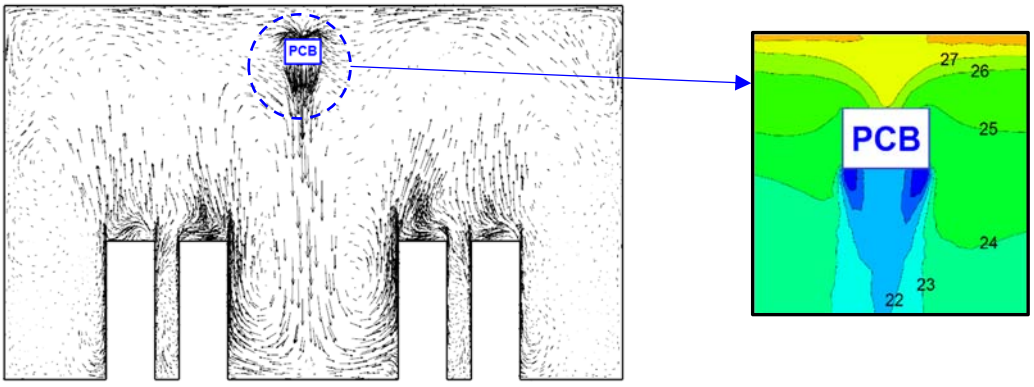

(a) Airflow pattern

(b) An example of the temperature contour near a PCB (unit: ^{o}C)

Fig. 6 Airflow and temperature development around a PCB

3.3 Thermal comfort analysis

In a room with a DV-PCB system, many parameters could affect thermal comfort. To study the effects of PCBs on thermal comfort in a DV system, this investigation simulated 14 cases with various parameters, as listed in Table 2. These cases were designed as follows. Cases 1-4 had the same high cooling load, supply air temperature and PCB type, while the overall percentage (η) of the load removed by the PCBs varied. Therefore, these four cases were used to study the cooling effect of the PCBs on indoor air and the influence of the PCB on the vertical temperature gradient, at different η. Section 3.3.1 presents the corresponding results. Cases 5-14 had the same medium cooling load and T_{sp} (air temperature at H=1.1m), but used different combinations of PCB types and different η. When type A or B was used, two pieces of PCB were installed in the mid-section of the room; when type C was used, three pieces were installed in parallel in the room. (Whether it was a 2-piece or 3-piece case, the cooling load removed by each piece was the overall cooling rate of all chilled beams divided by number of PCB pieces.)

Table 2. Parameters of the studied cases

Case #	Internal load Q (W/m^2)	PCB type and number	Percentage of load removed by PCBs (η)	T_s	Note
1	90	N/A	0%	21.0^{o}C	Used to study the impact of PCBs on the temperature gradient under a high cooling load
2	90	2B	40%		
3	90	2B	60%		
4	90	2B	80%		
5	61	N/A	0%	Adjusted so that T_{sp} = 23^{o}C	Used to study the impact of PCBs on the PD
6	61	2A	40%		

7	61	2A	60%	distribution under a medium cooling load
8	61	2A	80%	
9	61	2B	40%	
10	61	2B	60%	
11	61	2B	80%	
12	61	3C	40%	
13	61	3C	60%	
14	61	3C	80%	

3.3.1 Influence of PCBs on temperature gradient

One drawback of a DV system is that it may create a large temperature gradient in the occupied zone, which is not conducive to thermal comfort. Fig. 7 depicts the temperature profiles of three cases in which PCBs were used to remove different amounts of cooling load in the room, and illustrates how the PCB-induced cool jet changed the temperature profile. The results were obtained from a location in close proximity to an occupant.

In Case 1 (a case with 0% load removed by the PCBs), ΔT_{ha1} was larger than 3 K, and ΔT_{ha2} was larger than 4 K, both of which exceeded the temperature gradient limits set by ASHRAE [37]. While the PCBs were in operation, however, they significantly reduced the temperature gradient in the occupied zone, as shown in Cases 2 and 4. When the PCBs removed a small amount of heat in a room, they could reduce the temperature in the upper part of the room, as demonstrated by a comparison of Cases 1 and 2. In these two cases, the vertical temperature profiles in breathing zone were mainly dominated by the DV system, which was why their temperature profiles almost overlapped in lower part. When the cooling capacity of the PCBs was further increased (e.g. Case 4), they could also significantly decrease the temperature in the lower part of the room.

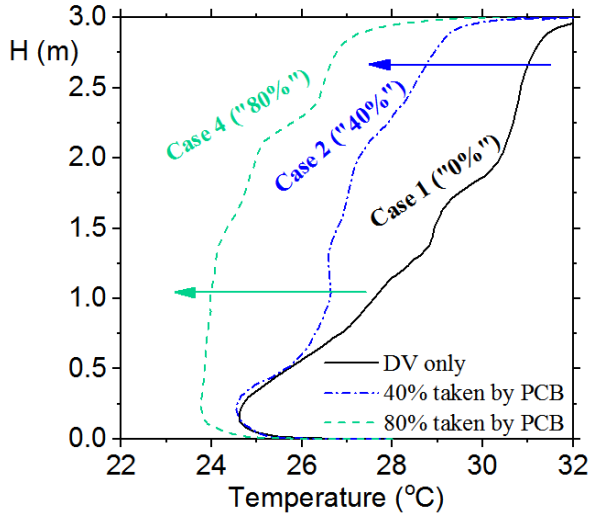

Fig. 7 Vertical temperature profiles when different percentages of cooling load were removed by PCBs

Fig. 8 compares the ΔT_{ha1} and ΔT_{ha2} under different η and ACH. The ΔT_{ha} was inversely correlated to η and ACH. When the cooling load was high, the DV-only system was not able to maintain a sufficiently small temperature gradient in the room, even when the air change rate was as large as ACH = 7.9. However, adding PCBs to the DV system could solve this problem. In a coupled DV-PCB system, the value of ΔT_{ha} results from combined effect of indoor space conditions, DV system parameters and PCB system parameters. Thus, a careful design should be implemented to ensure ΔT_{ha} meets the thermal comfort requirement.

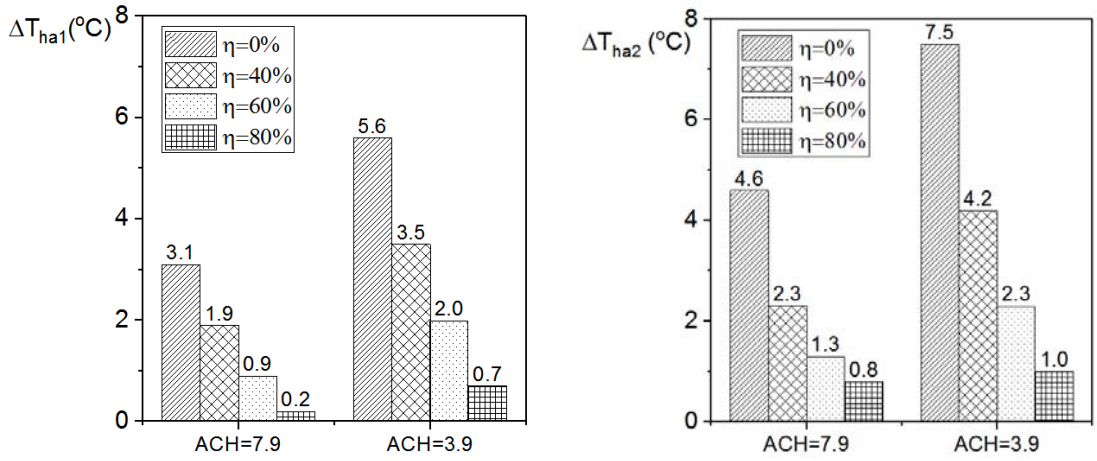

(a) $\Delta T_{ha1}(=T_{1.1\mathrm{m}}-T_{0.1\mathrm{m}})$ (b) $\Delta T_{ha2}(=T_{1.7\mathrm{m}}-T_{0.1\mathrm{m}})$

Fig. 8 Head-to-ankle temperature differences under different η and ACH

3.3.2 Draft in the coupled DV-PCB system

Although PCBs can reduce the room temperature gradient, the downward cold jet could increase the local percent dissatisfied. Fig. 9 compares the PD distributions for Case 5 (a DV-only system) and Case 10 (a DV-PCB system). The DV-only system had a low overall PD in the occupied zone. The added PCBs created a high-draft region beneath with a relatively low temperature, high air velocity, and PD > 15%. However, this region was observed only under the PCB, and the global PD remained the same.

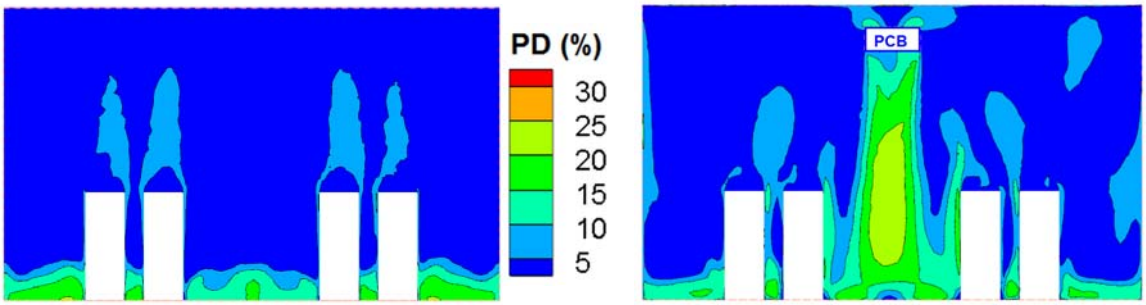

(a) Case 5 (DV-only system) (b) Case 10 (DV-PCB system)

Fig. 9 PD distribution at a vertical cross-section through dummies and PCB

Fig. 10 illustrates the change in PD with η beneath the PCB for the three sets of PCBs. With the same cooling load, the larger the η was, the higher the overall PD became. Although the standing and sitting heights differed by 0.6 m, the PD values at these two heights were comparable. Because jet flow in the region was still developing, the air temperature along the jet core did not change greatly. The PD at ankle level was much lower than that at standing or sitting heights, since the jet decayed significantly when it reached ankle level.

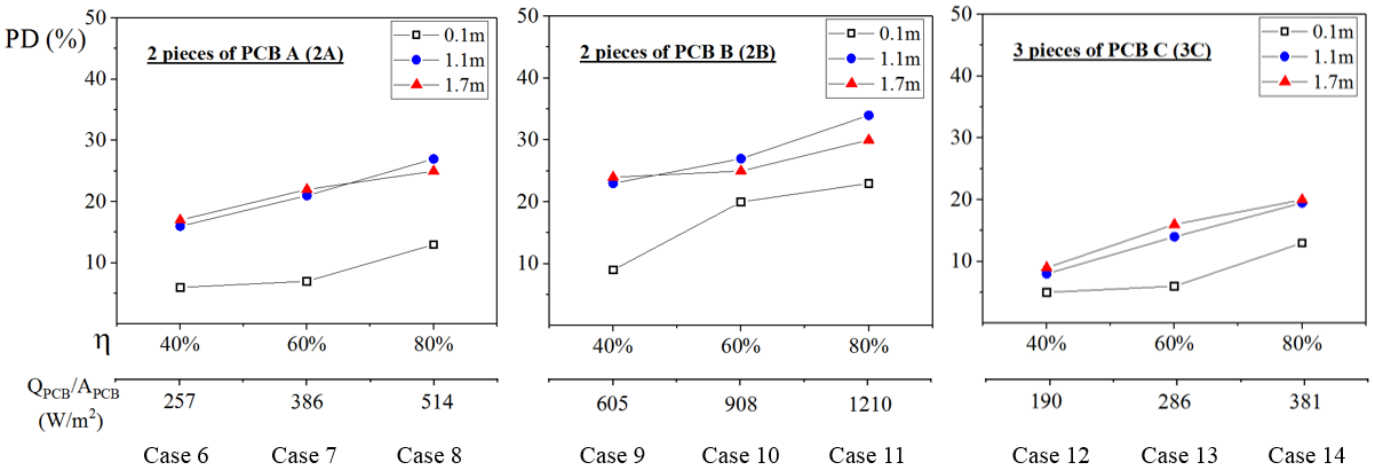

Fig. 10 PD at standing, siting and ankle heights under PCBs for different PCB configurations

Fig. 10 shows that when other parameters were the same, the PD under the PCBs increased when η increased. Furthermore, the PD under the PCBs was inversely correlated with the total cross-sectional area of the PCBs. For example, at η = 40% and H = 1.1 m, PD was the highest in the "2B" case and lowest in the "3C" case. The "3C" case had the largest PCB cross-sectional area and the "2B" case the smallest. These results occurred mainly because the strength of the downward jet increased with Q_{PCB}/A_{PCB} (total cooling load removed by PCB over total PCB cross-sectional area).

From indoor design perspective, Fig. 9 and Fig. 10 indicate that seats are suggested to be located at some distance away from PCB so that occupants could avoid high-draft region. Moreover, since the development of high-draft region, when obstructed by a table, is likely to propagate along table top surface, it is also not recommended to place tables away from PCB. However, as the high-draft region was restricted to be beneath PCB, PD level at most part of the room was satisfactory.

3.4 Impact of PCBs on indoor air quality

Figs. 12(a) and 12(b) depict the transport of gaseous contaminant in Case 5 (DV only) and Case 10 (DV-PCB) when the contaminant was released from a single source. In Case 5, the contaminant ascended with the thermal plume, which resulted in contaminant stratification. When PCBs were used, the downward jet recirculated the contaminant downward to the lower part of the room. The airflow pathlines in Figs. 12(a) and 12(b) also illustrated how PCB changed airflow pattern in the room. The normalized contaminant concentrations in Figs 12(c) and (d) very clearly show the impact of the PCBs on contaminant distribution. In the breathing zone, Case 5 exhibited much higher air quality than did Case 10. Actually, the contaminant concentration in the breathing zone in Case 10 was close to the perfectly mixed level (or the concentration at the exhaust).

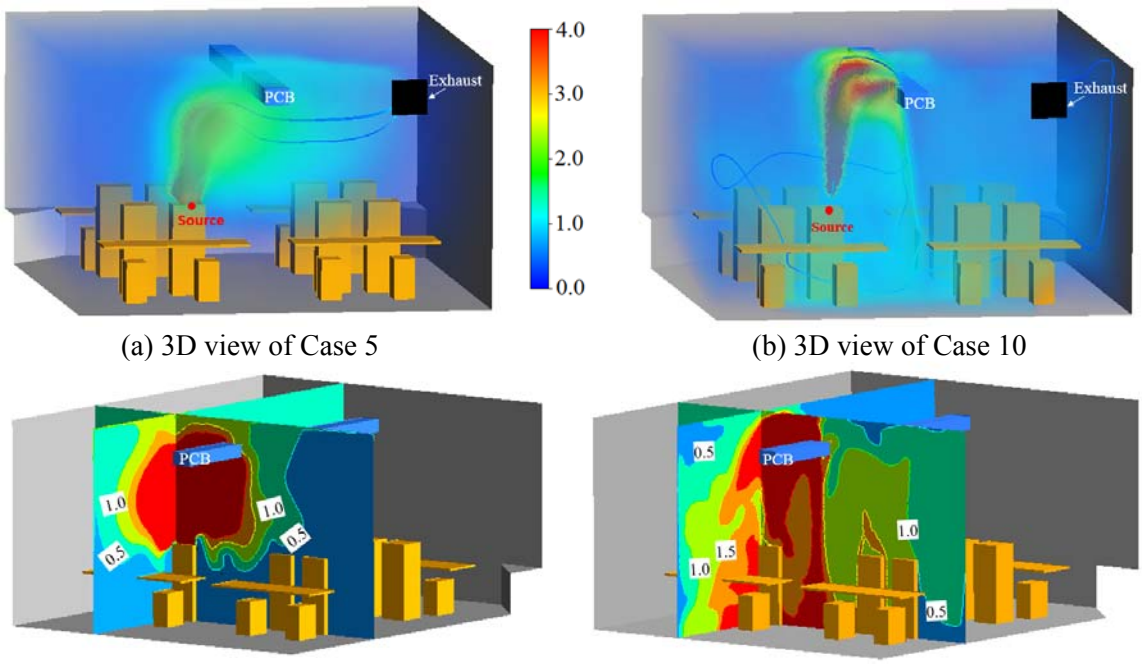

(a) 3D view of Case 5 (b) 3D view of Case 10

(c) Cross-sectional views of Case 5 (d) Cross-sectional views of Case 10

Fig. 11 Contaminant distributions in Case 5 (a DV-only case) and Case 10 (a DV-PCB case), where the contaminant concentration C^* was normalized by the exhaust concentration in (c) and (d).

The mean age of air (MAA) is another parameter that can be used to evaluate air quality. Fig. 12 shows the MAA distribution on a vertical cross section for the above two cases. Case 5 exhibited a significantly smaller MAA than Case 10, since much less air recirculation existed in Case 5. Under the same air change rate, the average MAAs at breathing height (1.1 m) in Case 5 and Case 10 were 351 s and 456 s, respectively. The corresponding MAA for perfect-mixing ventilation at this air change rate was 501 s. Therefore, the PCB greatly increased the MAA in the room by enhancing indoor air mixing. As a result, the high air change efficiency was negatively influenced by PCB. In the design of a DV-PCB system, it is important that suffcient fresh air is provided so that ventilation requirement could be met.

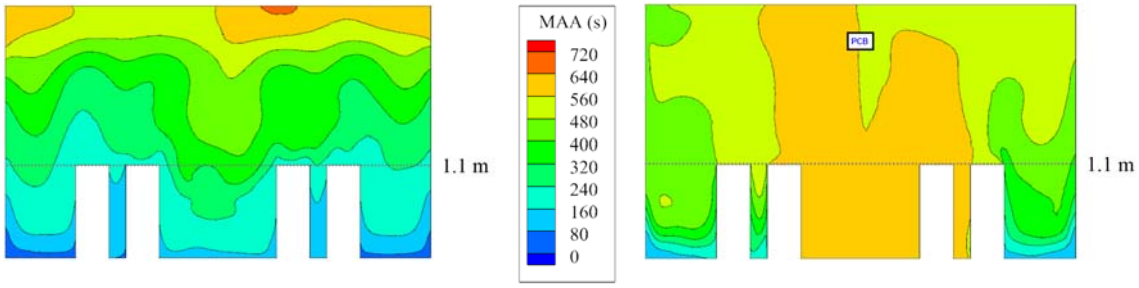

(a) Case 5 (b) Case 10

Fig. 12 Local mean age of air (MAA) in Cases 5 and 10

4. Discussion

4.1 Evaluation of thermal comfort using PD

This study used PD to evaluate thermal comfort. Although it is a widely accepted index, PD was

developed for the entire body. Our study used it to assess local thermal comfort, which may have led to some errors. However, since a significant spatial variation in PD distribution was observed in the room with the DV-PCB system (as shown in Fig. 9), the local PD distribution provided more comprehensive draft-related thermal comfort information than would a single average PD value. Moreover, the local distribution provided valuable information for indoor air distribution design. For example, because a "zone with high draft" was found beneath the PCBs, it is recommended that seats or desks not be placed directly under PCBs. In fact, many previous studies have also used PD to evaluate local thermal comfort, either to evaluate the performance of a system [57, 58] or to guide the design of an indoor space [59]. Therefore, we believe that PD can be used for evaluating local thermal comfort.

4.2 Spatial distribution of predicted mean vote (PMV)

PMV is a widely used scale that quantifies thermal comfort into 7 levels based on the energy balance of body [40]. Fig. 13(a) demonstrates PMV distribution (at clothing level $I_{cl} = 0.8$) in a vertical cross section in Case 4, where a very large cooling capacity of PCBs was used. Results showed that while the overall PMV level in the room was around 0, right beneath PCB there existed a band where PMV was -1. It suggests that when most region in the room gives neutral predicted thermal sensation, occupants will feel slightly cool under PCB. Fig. 13(b) further plots the distribution of PPD, percentage predicted dissatisfied people [40] for the same case. In most of the room space, the PPD level was under 10%, but the PPD magnitude could be as large as 30% beneath PCB. Results indicated that the impact of PCB on the PMV and PPD distributions was mainly in the zone right beneath PCB. It should be noted that one can always adjust the clothing level to adjust the PMV and PPD results. However, these results still illustrated clearly the spatial variation of predicted thermal sensation level in a DV-PCB system.

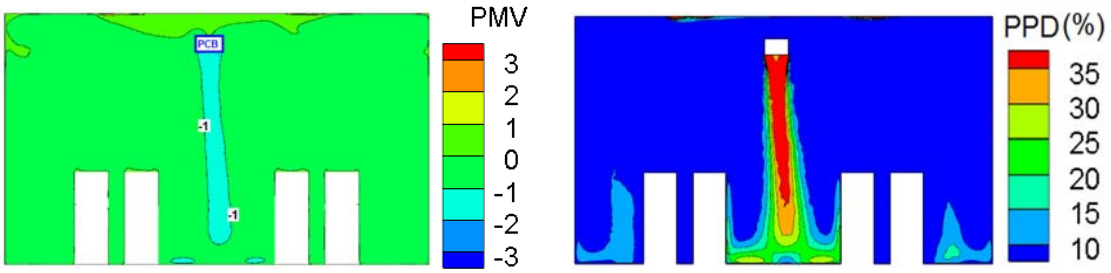

(a) PMV (b) PPD

Fig. 13 PMV and PPD distributions in Case 4

4.3 Impact of room layout

This study primarily used an office layout to analyze the performance of the DV-PCB system. In practice room layouts vary and can include classrooms and conference rooms (Fig. 2). Fig. 14 compares temperature distributions in the three different room layouts under the same cooling load (61 W/m^2), same supply air temperature (18.5 ^{o}C), and same air flow rate. PCBs were not used because they would have added another level of complexity. Although the local air distribution could vary, quite similar temperature profiles were observed for these three cases. This finding agrees with those in previous studies [60, 61] which indicated that the heat source arrangement in the occupied zone has little impact on the overall temperature and airflow distribution in a room. Therefore, the thermal and ventilation assessments of the DV-PCB system in this study will still be valid if the room layout changes.

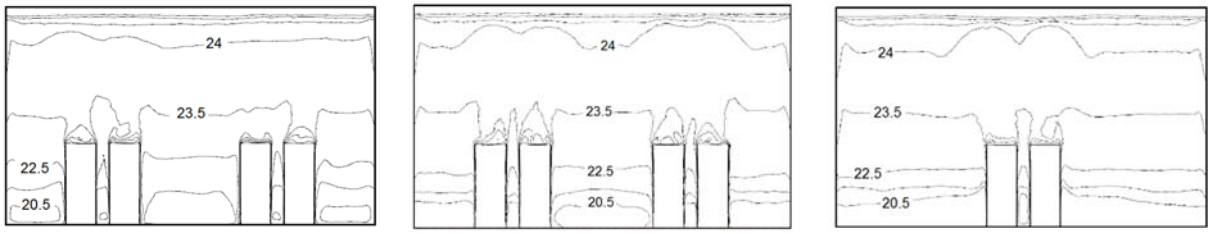

(a) Office (b) Classroom (c) Conference Room

Fig. 14 Comparison of temperature contours for three room layouts (unit: ^{o}C)

4.4 Limitations and future study

There are several limitations in this investigation. First, the current research assumed the indoor space is well sealed, so air enters the room entirely from diffusers and leaves the room through exhaust. This should be valid for a lot of indoor spaces because of the enhanced sealing technologies implemented in today's buildings. Nevertheless, in scenarios where major openings (revolving doors, open windows etc.) exist, air from these openings might affect the indoor airflow and contaminant distribution that are developed by DV-PCB system. Second, a lot of the results in this study were obtained from CFD model. From Fig. 5, it can be noticed that CFD results deviates from measurement data at some locations, especially at Pole 5 of contaminant concentration. Hence, CFD analysis does not fully resolve the airflow physics in the room and might lead to some errors. However, since the developed CFD model captured the airflow and contaminant concentration trends with good accuracy, as discussed in Section 3.1, the conclusions drawn based on CFD analysis are plausible.

This research studied thermal comfort and air quality in a room with a DV-PCB system. In order to design a DV-PCB system that meets thermal and ventilation requirements, future study needs to be performed to establish design guidelines. This involves further analysis of thermal comfort and air quality in occupied zone based on various parameters including cooling load, air change rate, whether the indoor space has a façade etc. In addition, chilled ceiling is also widely used in high-cooling load applications, and the physics for its cooling is different than that of passive chilled beams. It is thus beneficial to perform a comparative study by replacing the PCBs in current study with chilled ceilings and to investigate the differences. Finally, the experiments in current study were performed in an environmental chamber. Although the conditions in the chamber were set up to be as close to reality as possible, it will be valuable to conduct further experiments and analyses in an actual indoor space that has a DV-PCB system.

5. Conclusions

This study used experimental measurements and CFD simulations to investigate indoor airflow and contaminant concentration in a room with a coupled DV-PCB system. The CFD model was also used to evaluate thermal comfort and indoor air quality. The study led to following conclusions:

(1) This investigation constructed a DV-PCB system in a full-scale environmental chamber and measured the profiles of air velocity, temperature and contaminant concentration in multiple locations in the chamber for validation of the CFD model. A comparison of the simulated results and the measured data showed that the CFD model can predict indoor airflow and contaminant transport in the chamber with good accuracy.
(2) When the cooling load is high, a DV-only system could create a high temperature gradient between head and ankle levels, which may cause discomfort. However, passive chilled beams

were found to effectively reduce the temperature gradient if the PCBs were used to remove 40% or more of the cooling load.

(3) The PCB-induced cold jet produced a high-draft region (PD > 15%) beneath the PCBs. The PD under the PCBs was positively correlated with the amount of heat removed by the PCBs, but inversely correlated with the total cross-sectional area of PCBs. The high-draft region was observed only under the PCBs, and the global PD level remained unaffected.

(4) The PCBs caused an airborne contaminant near the ceiling to travel downward to the occupied zone, thus disrupting the contaminant stratification created by DV. If the PCB-induced downward jet was strong enough, the contaminant concentration at breathing height could be similar to that with mixing ventilation. The PCBs also increased the mean age of air in the room.

(5) This study assumes that the diffusers and exhausts are the only airflow inlets and outlets, respectively, of the indoor space. Although air leakage from doors or windows can be minimal due to advanced sealing technology, airflow from major openings (revolving doors etc.), if applicable, might affect the indoor airflow pattern and contaminant distribution that are developed by a DV-PCB system. Future research opportunities include development of a design guideline for DV-PCB systems, investigating impact of different openings on DV-PCB system and comparison of impacts of PCB and chilled ceiling on DV systems.

Acknowledgement

The authors are grateful for the support by American Society of Heating, Refrigerating and Air-conditioning Engineers (ASHRAE) on this research through research project 1666.

References

[1] Akimoto, T., Tanabe, S. I., Yanai, T., & Sasaki, M. (2010). Thermal comfort and productivity-Evaluation of workplace environment in a task conditioned office. Building and Environment, 45(1), 45-50.

[2] Xing, H., & Awbi, H. B. (2002). Measurement and calculation of the neutral height in a room with displacement ventilation. Building and Environment, 37(10), 961-967.

[3] Gilani, S., Montazeri, H., & Blocken, B. (2016). CFD simulation of stratified indoor environment in displacement ventilation: Validation and sensitivity analysis. Building and Environment, 95, 299-313.

[4] Mateus, N. M., & da Graça, G. C. (2017). Simulated and measured performance of displacement ventilation systems in large rooms. Building and Environment, 114, 470-482.

[5] Chen, Q., & Glicksman, L. (2003). System performance evaluation and design guidelines for displacement ventilation[prepared under ASHRAE research project 949]. American Society of Heating, Refrigerating, and Air-Conditioning Engineers, Incorporated.

[6] Lin, Z., Lee, C. K., Fong, S., Chow, T. T., Yao, T., & Chan, A. L. S. (2011). Comparison of annual energy performances with different ventilation methods for cooling. Energy and Buildings, 43(1), 130-136.

[7] Ahmed, A. Q., Gao, S., & Kareem, A. K. (2016). A numerical study on the effects of exhaust locations on energy consumption and thermal environment in an office room served by displacement ventilation. Energy Conversion and Management, 117, 74-85.

[8] Cheng, Y., Niu, J., Liu, X., & Gao, N. (2013). Experimental and numerical investigations on stratified air distribution systems with special configuration: Thermal comfort and energy saving. Energy and Buildings, 64, 154-161.

[9] Schultz, R. (2012). When, where to use displacement ventilation? Retrieved from https://www.csemag.com/articles/when-where-to-use-displacement-ventilation/

[10] Titus HVAC. (2013). Displacement Ventilation Catalog Section. Retrieved from: https://www.titus-hvac.com/docs/2014%20catalog/displacement_2013.pdf

[11] Burt, L. W. (2007). Life cycle cost of displacement ventilation in an office building with a hot and humid climate (Doctoral dissertation, University of Florida).

[12] ASHRAE, U. (2013). Guide: Design, Construction and Operation of Underfloor Air Distribution Systems. American Society of Heating, Refrigerating and Air-Conditioning Engineers, Atlanta, GA.

[13] Lau, J., & Chen, Q. (2006). Energy analysis for workshops with floor–supply displacement ventilation under the US climates. Energy and Buildings, 38(10), 1212-1219.

[14] Alain, M., Kamel, G., & Nesreen, G. (2012). A simplified combined displacement and personalized ventilation model. HVAC&R Research, 18(4), 737-749.

[15] Rees, S. J., & Haves, P. (2013). An experimental study of air flow and temperature distribution in a room with displacement ventilation and a chilled ceiling. Building and Environment, 59, 358-368.

[16] Hao, X., Zhang, G., Chen, Y., Zou, S., & Moschandreas, D. J. (2007). A combined system of chilled ceiling, displacement ventilation and desiccant dehumidification. Building and Environment, 42(9), 3298-3308.

[17] Causone, F., Baldin, F., Olesen, B. W., & Corgnati, S. P. (2010). Floor heating and cooling combined with displacement ventilation: Possibilities and limitations. Energy and Buildings, 42(12), 2338-2352.

[18] Loudermilk, K. (2009). Designing chilled beams for thermal comfort. ASHRAE Journal, 51(10), 58-63.

[19] Koskela, H., Häggblom, H., Kosonen, R., & Ruponen, M. (2010). Air distribution in office environment with asymmetric workstation layout using chilled beams. Building and Environment, 45(9), 1923-1931.

[20] Rhee, K. N., Shin, M. S., & Choi, S. H. (2015). Thermal uniformity in an open plan room with an active chilled beam system and conventional air distribution systems. Energy and Buildings, 93, 236-248.

[21] Nelson, I. C., Culp, C. H., Rimmer, J., & Tully, B. (2016). The effect of thermal load configuration on the performance of passive chilled beams. Building and Environment, 96, 188-197.

[22] Fong, K. F., Chow, T. T., Lee, C. K., Lin, Z., & Chan, L. S. (2011). Solar hybrid cooling system for high-tech offices in subtropical climate–Radiant cooling by absorption refrigeration and desiccant dehumidification. Energy Conversion and Management, 52(8-9), 2883-2894.

[23] Fredriksson, J., & Sandberg, M. (2009). The effect of false ceiling on the cooling capacity of passive chilled beams. Building and Environment, 44(7), 1426-1430.

[24] Kim, J., Braun, J. E., & Tzempelikos, A. (2014). Energy savings potential of passive chilled beam system as a retrofit option for commercial buildings in different climates. Proceedings of the 3rd International High Performance Building Conference, West Lafayette, Indiana, USA.

[25] Rumsey, P., & Weale, J. (2007). Chilled beams in labs: Eliminating reheat & saving energy on a budget. ASHRAE Journal, 49(1), 18.

[26] TIAX LLC. (2002). Energy Consumption Characteristics of Commercial Building HVAC Systems—Volume III: Energy Savings Potential. Final Report to U.S. Department of Energy, Office of Building Technologies. Retrieved from: https://www1.eere.energy.gov/buildings/publications/pdfs/commercial_initiative/hvac_volu me3_final_report.pdf

[27] Roth, K., Dieckmann, J., Zogg, R., & Brodrick, J. (2007). Chilled beam cooling. ASHRAE Journal, 49(9), 84-86.

[28] Fredriksson, J., Sandberg, M., & Moshfegh, B. (2001). Experimental investigation of the velocity field and airflow pattern generated by cooling ceiling beams. Building and environment, 36(7), 891-899.

[29] Kosonen, R., Saarinen, P., Koskela, H., & Hole, A. (2010). Impact of heat load location and strength on air flow pattern with a passive chilled beam system. Energy and Buildings, 42(1), 34-42.

[30] Riffat, S. B., Zhao, X., & Doherty, P. S. (2004). Review of research into and application of chilled ceilings and displacement ventilation systems in Europe. International Journal of Energy Research, 28(3), 257-286.

[31] Lee, K., Zhang, T., Jiang, Z., & Chen, Q. (2009a). Comparison of airflow and contaminant distributions in rooms with traditional displacement ventilation and under-floor air distribution systems. ASHRAE Transactions, 115(2), 306-321.

[32] Lee, S. C., & Wang, B. (2006). Characteristics of emissions of air pollutants from mosquito coils and candles burning in a large environmental chamber. Atmospheric Environment, 40(12), 2128-2138.

[33] Buratti, C., Palladino, D., & Moretti, E. (2017). Prediction Of Indoor Conditions And Thermal Comfort Using CFD Simulations: A Case Study Based On Experimental Data. Energy Procedia, 126, 115-122.

[34] Shi, Z., Chen, J., You, R., Chen, C., & Chen, Q. (2016). Modeling of gasper-induced jet flow and its impact on cabin air quality. Energy and Buildings, 127, 700-713.

[35] Barbosa, B. P. P., & Brum, N. D. C. L. (2018). Validation and assessment of the CFD-0 module of CONTAM software for airborne contaminant transport simulation in laboratory and hospital applications. Building and Environment, 142, 139-152.

[36] Van Hooff, T., & Blocken, B. (2016). CFD simulations of mixing ventilation at low Reynolds numbers: effect of spatial discretization scheme. In 14th International Conference on Indoor Air Quality and Climate (Indoor Air 2016), July 3-8, 2016, Ghent, Belgium.

[37] Sadrizadeh, S., & Ploskic, A. (2016). On the boundary conditions of numerical particle simulation in indoor environment. In Proc. 14th Int. Conf. Indoor Air Qual. Clim.

[38] Rai, A. C., Lin, C. H., & Chen, Q. (2014). Numerical modeling of volatile organic compound emissions from ozone reactions with human-worn clothing in an aircraft cabin. HVAC&R Research, 20(8), 922-931.

[39] Chen, C., & Zhao, B. (2017). A modified Brownian force for ultrafine particle penetration through building crack modeling. Atmospheric environment, 170, 143-148.

[40] Coleman, H. W., & Stern, F. (1997). Uncertainties and CFD code validation. Journal of Fluids Engineering, 119(4), 795-803.

[41] Lau, J., & Chen, Q. (2007). Floor-supply displacement ventilation for workshops. Building and Environment, 42(4), 1718-1730.

[42] LumaSense Technologies. (2017). INNOVA 1309 User Manual. Retrieved from https://innova.lumasenseinc.com/manuals/historical-manuals/1309/

[43] LumaSense Technologies. (2017). INNOVA 1312 User Manual. Retrieved from https://innova.lumasenseinc.com/manuals/historical-manuals/1312/

[44] Yakhot, V. S. A. S. T. B. C. G., Orszag, S. A., Thangam, S., Gatski, T. B., & Speziale, C. G. (1992). Development of turbulence models for shear flows by a double expansion technique. Physics of Fluids A: Fluid Dynamics, 4(7), 1510-1520.

[45] Zhang, Z., Zhang, W., Zhai, Z. J., & Chen, Q. Y. (2007). Evaluation of various turbulence models in predicting airflow and turbulence in enclosed environments by CFD: Part 2—Comparison with experimental data from literature. HVAC&R Research, 13(6), 871-886.

[46] ANSYS Inc. (2016). ANSYS Fluent Theory Guide 17.0. Canonsburg, PA.

[47] Fadhl, B., Wrobel, L. C., & Jouhara, H. (2013). Numerical modelling of the temperature distribution in a two-phase closed thermosyphon. Applied Thermal Engineering, 60(1-2), 122-131.

[48] Olesen, B. W., Scholer, M., & Fanger, P. O. (1979). Discomfort caused by vertical air temperature differences. Indoor Climate, 36, 561-578.

[49] Ilmarinen, R., Palonen, J., & Seppänen, O. (1992). Effects of non-uniform thermal conditions on body temperature responses in women. Proceedings of the 41st Nordiska Arbetsmiljömötet, 181-182.

[50] Schellen, L., Loomans, M. G., de Wit, M. H., Olesen, B. W., & van Marken Lichtenbelt, W. D. (2012). The influence of local effects on thermal sensation under non-uniform environmental conditions—Gender differences in thermophysiology, thermal comfort and productivity during convective and radiant cooling. Physiology & behavior, 107(2), 252-261.

[51] ASHRAE, A., & Standard, A. S. H. R. A. E. (2013). 55 2013. Thermal Environmental Conditions for Human Occupancy, American Society of Heating, Ventilating and Air-conditioning Engineers, Atlanta.

[52] Fanger, P. O. (1970). Thermal comfort. Analysis and applications in environmental engineering. Thermal Comfort. Analysis and Applications in Environmental Engineering. Copenhagen: Danish Technical Press.

[53] Fleming, K. K., Longmire, E. K., & Hubel, A. Numerical characterization of diffusion-based extraction in cell-laden flow through a microfluidic channel. Journal of Biomechanical Engineering 129, no. 5 (2007): 703-711.

[54] Li, X., Li, D., Yang, X., & Yang, J. (2003). Total air age: An extension of the air age concept. Building and Environment, 38(11), 1263-1269.

[55] Pope, S. B. (2000). Turbulent Flows. Cambridge: Cambridge University Press.

[56] Gurevich, M. I. (2014). The Theory of Jets in an Ideal Fluid (Vol. 93). Elsevier.

[57] Xu, H. T., & Niu, J. L. (2003, August). A new method of CFD simulation of airflow characteristics of swirling floor diffusers. In Proc Building Simulation (Vol. 3, pp. 1429-1434).

[58] You, R., Zhang, Y., Zhao, X., Lin, C. H., Wei, D., Liu, J., & Chen, Q. (2018). An innovative personalized displacement ventilation system for airliner cabins. Building and Environment, 137, 41-50.

[59] Wang, Y., Lian, Z., Broede, P., & Lan, L. (2012). A time-dependent model evaluating draft in indoor environment. Energy and Buildings, 49, 466-470.

[60] Melhado, M. A., Beyer, P. O., Hensen, J. M., & Siqueira, L. F. G. (2005). The thermal comfort, the indoor environment control, and the energy consumption in three types of operating rooms. Surgeon, 230(50), 0-90.

[61] Lee, K. Jiang, Z., & Chen, Q. (2009b). Air distribution effectiveness with stratified air distribution systems. ASHRAE Transactions, 115, 322.